

Phase-Consistent Magnetic Spectral Learning for Multi-View Clustering

Mingdong Lu, Zhikui Chen, Meng Liu, Shubin Ma, Liang Zhao

School of Software, Dalian University of Technology

{mingdonglu, liumeng, shubinma}@mail.dlut.edu.cn, {zkchen, liangzhao}@dlut.edu.cn

Abstract

Unsupervised multi-view clustering (MVC) aims to partition data into meaningful groups by leveraging complementary information from multiple views without labels, yet a central challenge is to obtain a reliable shared structural signal to guide representation learning and cross-view alignment under view discrepancy and noise. Existing approaches often rely on magnitude-only affinities or early pseudo targets, which can be unstable when different views induce relations with comparable strengths but contradictory directional tendencies, thereby distorting the global spectral geometry and degrading clustering. In this paper, we propose *Phase-Consistent Magnetic Spectral Learning* for MVC: we explicitly model cross-view directional agreement as a phase term and combine it with a nonnegative magnitude backbone to form a complex-valued magnetic affinity, extract a stable shared spectral signal via a Hermitian magnetic Laplacian, and use it as structured self-supervision to guide unsupervised multi-view representation learning and clustering. To obtain robust inputs for spectral extraction at scale, we construct a compact shared structure with anchor-based high-order consensus modeling and apply a lightweight refinement to suppress noisy or inconsistent relations. Extensive experiments on multiple public multi-view benchmarks demonstrate that our method consistently outperforms strong baselines.

1 Introduction

Unsupervised multi-view clustering aims to partition data into semantically meaningful clusters by exploiting complementary information from multiple views, without requiring manual annotations. Such multi-view observations widely arise in practice, e.g., multi-sensor measurements or heterogeneous feature extractors of the same data. While multi-view learning can improve robustness via cross-view complementarity, achieving *consistent* and *robust* clustering in the unsupervised setting remains challenging.

A common thread behind existing MVC approaches is

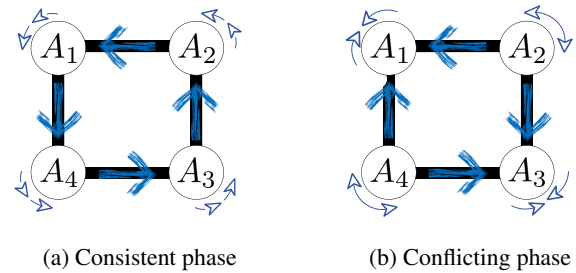


Figure 1: **Phase effects beyond affinity magnitude.** With identical affinity magnitudes, consistent directions yield a coherent flow and a stable global structure, whereas conflicting directions cancel out and induce a different spectrum.

to infer a *shared clustering structure* (e.g., a shared embedding/graph or pseudo targets) across views and use it to guide representation learning and fusion [Zhou *et al.*, 2024; Fang *et al.*, 2023]. However, in real-world multi-view data, noise, view discrepancy, and structural conflicts can make such shared signals unreliable. When pseudo targets or structural cues are inaccurate, directly enforcing strong cross-view alignment may amplify errors and cause supervision drift or mismatched alignment [Xu *et al.*, 2024; Arazo *et al.*, 2020; Gao *et al.*, 2024]. Therefore, constructing a reliable shared structural signal under view conflicts and turning it into stable learning supervision remains a key bottleneck for unsupervised MVC.

More importantly, instability does not necessarily manifest as weak connections. Beyond connection strength (magnitude), cross-view relations may exhibit *directional tendencies* whose agreement can substantially affect global spectral behavior. Here the “direction” is not intrinsic to the original undirected affinity, but an emergent proxy of cross-view disagreement (e.g., view-induced preferences in mapping samples to anchors), which can be encoded as a phase term. This is consistent with directed-graph and connection-Laplacian spectral theories [Chung, 2005; Singer and Wu, 2012; Liu *et al.*, 2026], and magnetic (complex-valued) Laplacians that incorporate phase/direction to characterize directed-network structures [Fanuel *et al.*, 2017]. As illustrated in Fig. 1, even under identical affinity magnitudes, consistent directions yield a coherent flow and a stable spectrum, whereas conflicting directions can cancel out and induce a markedly different

spectrum. This motivates us to model not only magnitude but also cross-view *directional consistency* when constructing shared structural signals for MVC.

To address these challenges, we propose *Phase-Consistent Magnetic Spectral Learning* for unsupervised MVC. We construct a nonnegative magnitude backbone as a stable shared geometry, encode cross-view directional agreement as a phase term to form a magnetic affinity, and extract a shared spectral signal via a Hermitian magnetic Laplacian to provide structured self-supervision for multi-view representation learning. For scalable and robust structure estimation, we employ an anchor-based high-order consensus model (anchor hypergraph) and an efficient refinement to suppress noisy or inconsistent relations before phase estimation and spectral extraction.

Our main contributions are summarized as follows:

- We propose *phase-consistent magnetic spectral learning* for unsupervised MVC by jointly modeling magnitude and cross-view directional agreement, and deriving a stable shared spectral signal via a Hermitian magnetic Laplacian for structured self-supervision.
- We develop an *anchor-hypergraph* based structure construction that preserves high-order cross-view consensus while enabling spectral learning in a compact anchor domain, together with an efficient refinement for robust phase estimation and spectral extraction.
- Experiments on ten public multi-view benchmarks show consistent improvements over strong baselines, with ablations and analyses validating the effectiveness of phase consistency, structure construction/refinement, and the learning objectives.

2 Related Work

Unsupervised multi-view clustering. Unsupervised MVC aims to uncover a shared clustering structure from multiple views without labels. Classical studies often couple view-wise spectral embeddings or subspace models via co-regularization to encourage consensus [Kumar *et al.*, 2011]. Recent advances increasingly adopt deep encoders to learn view-specific representations via self-training [Xie *et al.*, 2016; Guo *et al.*, 2017; Pan *et al.*, 2021; Xu *et al.*, 2022; Cui *et al.*, 2024; Chen *et al.*, 2023], while graph-based MVC explores fusing shared (bi)partite graphs to better capture cluster geometry [Kang *et al.*, 2020; Li *et al.*, 2015; Zhang *et al.*, 2024; Wang *et al.*, 2025; Cui *et al.*, 2023]. A recurring challenge is that pseudo targets and shared structural cues can be unreliable under noise or view discrepancy, prompting growing attention toward robust, uncertainty-aware self-supervision [Arazo *et al.*, 2020; Xu *et al.*, 2024; Hu *et al.*, 2025].

Scalable structure construction with anchors and hypergraphs. To scale spectral learning beyond $O(n^2)$, landmark/anchor representations compress the data manifold using sparse associations [Chen and Cai, 2011; Li *et al.*, 2015; Zhang *et al.*, 2024; Wang *et al.*, 2025] and have been widely integrated with bipartite-graph learning to improve efficiency and robustness [Li *et al.*, 2015; Cui *et al.*, 2023;

Symbol	Meaning
V, n, K	#views, #samples, #clusters
$X^{(v)}, Z^{(v)}$	input data and latent codes of view v
d	latent dimension
m	#anchors (per view unless specified)
$A^{(v)}$	latent anchor centers of view v
$C^{(v)}$	sample-anchor coefficients of view v
H	anchor hypergraph incidence matrix ($m \times n$)
w, κ	hyperedge weights; curvature reweighting
S'	curvature-refined anchor affinity (anchor graph)
$\tilde{A}, L_{\text{mag}}$	magnetic adjacency and Laplacian on anchors
U	sample-level spectral embedding
$Q^{(v)}, P$	per-view soft assignments; shared targets

Table 1: Notation for the main geometric and spectral components.

Zhang *et al.*, 2024; Wang *et al.*, 2025]. Hypergraph modeling further generalizes pairwise graphs by encoding high-order relations, offering a natural tool to represent groupwise consistency patterns [Zhou *et al.*, 2006; Feng *et al.*, 2019; Zeng *et al.*, 2026; Gu and Wang, 2025]. These scalable constructions are closely related to ours, but existing pipelines are typically magnitude-centric and do not explicitly expose cross-view *directional agreement* as a spectral signal.

Geometry refinement and phase-aware spectral learning. Graph/hypergraph refinement via curvature or Ricci-style reweighting has been explored to suppress noisy connections and stabilize the induced geometry [Ollivier, 2009; Sia *et al.*, 2019; Ni *et al.*, 2019]. On the spectral side, directed/connection-based theories show that orientation information can fundamentally change the spectrum and embeddings [Chung, 2005; Singer and Wu, 2012]. Magnetic (complex-valued) Laplacians provide a principled way to encode direction/phase on edges while retaining Hermitian spectral properties [Faniel *et al.*, 2017; de Resende and Costa, 2020; Fiorini *et al.*, 2023; Lin and Gao, 2023; Hirn *et al.*, 2021]. Different from prior uses mainly targeting directed networks, we leverage a phase-consistent magnetic spectrum as *structured self-supervision* for MVC, extracted on a compact anchor-based high-order structure and coupled with geometry-aware learning objectives.

3 Method

Problem statement. We study unsupervised multi-view clustering. Given V views of the same n samples, $\{X^{(v)}\}_{v=1}^V$, the goal is to partition the samples into K clusters by learning view-specific latent representations $\{Z^{(v)}\}$ and, crucially, constructing a reliable *shared structural signal* across views to guide representation learning and cross-view alignment. The key symbols used in this section are summarized in Table 1.

Method overview. Motivated by the instability of shared structure under view discrepancy and noise, we build a compact shared geometric backbone in the latent space and then progressively turn it into stable training signals. Specifically, we first learn view-wise latent codes and construct an anchor hypergraph as a scalable magnitude backbone, which will be

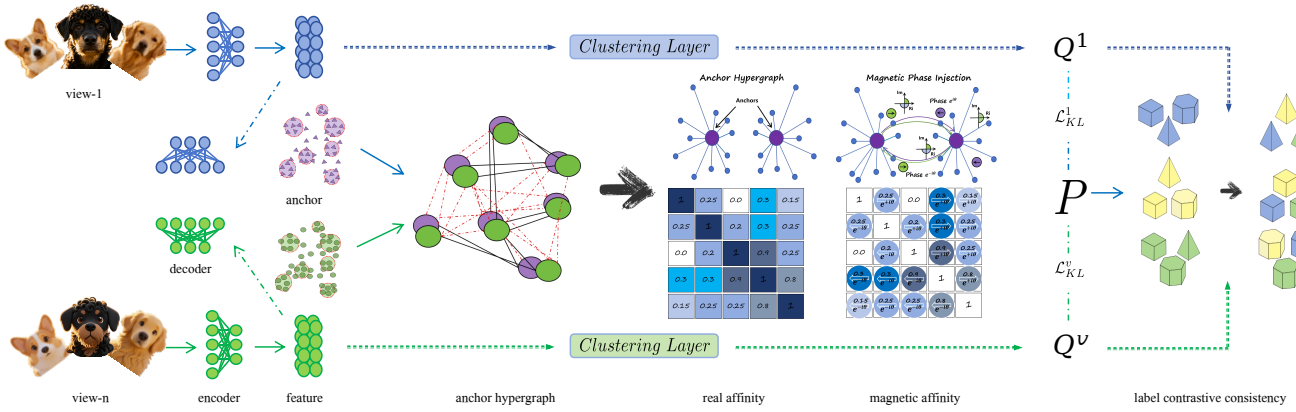


Figure 2: **Overall framework of Phase-Consistent Magnetic Spectral Learning for MVC.** Each view is encoded into latent features with reconstruction learning. View-wise latent anchors induce sparse sample–anchor relations, which are aggregated into a multi-view anchor hypergraph to form a compact shared magnitude backbone. We stabilize the backbone by refining hyperedge weights via curvature/Ricci-flow reweighting, then encode cross-view directional agreement as a magnetic (phase) term and extract a shared spectral signal using a Hermitian magnetic Laplacian. The resulting signal defines a global target distribution P to supervise per-view predictions $Q^{(v)}$ via KL alignment, while label contrastive consistency further reduces cross-view mismatch for robust clustering.

refined and later augmented with phase information for magnetic spectral signal extraction as illustrated in Figure 2.

3.1 Multi-view Autoencoders and Anchor Hypergraph Construction

Multi-view autoencoders. For each view $v \in \{1, \dots, V\}$, we learn an encoder–decoder pair $(f_\phi^{(v)}, g_\psi^{(v)})$ to obtain latent codes and reconstructions:

$$z_i^{(v)} = f_\phi^{(v)}(x_i^{(v)}), \quad \hat{x}_i^{(v)} = g_\psi^{(v)}(z_i^{(v)}), \quad (1)$$

where $x_i^{(v)} \in \mathbb{R}^{d_v}$ and $z_i^{(v)} \in \mathbb{R}^d$. We pretrain the autoencoders with the standard reconstruction objective

$$\mathcal{L}_{\text{rec}} = \sum_{v=1}^V \|X^{(v)} - \hat{X}^{(v)}\|_F^2. \quad (2)$$

Anchor-based subspace representation. To obtain a compact latent geometry, we summarize each view by m_v latent anchors $A^{(v)} \in \mathbb{R}^{d \times m_v}$, initialized by running k -means on $\{z_i^{(v)}\}_{i=1}^{n_v}$. Each latent code is approximated by a convex combination of anchors, $z_i^{(v)} \approx A^{(v)}c_i^{(v)}$, where $c_i^{(v)} \in \mathbb{R}^{m_v}$ is obtained by a simplex-constrained quadratic program:

$$\min_{c_i^{(v)} \geq 0, \mathbf{1}^\top c_i^{(v)} = 1} \|z_i^{(v)} - A^{(v)}c_i^{(v)}\|_2^2 + \gamma \|c_i^{(v)}\|_2^2. \quad (3)$$

Stacking $\{c_i^{(v)}\}_{i=1}^{n_v}$ as columns forms $C^{(v)} \in \mathbb{R}^{m_v \times n}$.

Anchor hypergraph construction. We aggregate all views by concatenating the coefficient matrices along the anchor dimension: $C^{\text{mv}} = \text{Concat}_{v=1}^V(C^{(v)}) \in \mathbb{R}^{m \times n}$ with $m = \sum_{v=1}^V m_v$. For each sample i , we keep only the r largest entries in the i -th column of C^{mv} (across all anchors and views) to obtain the anchor hypergraph incidence matrix $H \in \mathbb{R}^{m \times n}$:

$$H(:, i) = \mathcal{T}_r(C^{\text{mv}}(:, i)), \quad i = 1, \dots, n, \quad (4)$$

where $\mathcal{T}_r(\cdot)$ denotes column-wise Top- r sparsification. Each column $H(:, i)$ defines a hyperedge associated with sample i . We initialize hyperedge weights with $w^{(0)} = \mathbf{1} \in \mathbb{R}^n$; the resulting $(H, w^{(0)})$ will be refined by curvature-driven reweighting and used as the shared geometric backbone in the sequel.

3.2 Phase-Consistent Magnetic Spectral Signal and Self-supervision

Curvature-based refinement of the anchor hypergraph. Given the anchor hypergraph $(H, w^{(0)})$ (Sec. 3.1), we assign each hyperedge e (sample) a discrete curvature κ_e from its local incidence pattern and update hyperedge weights by a curvature-driven discrete Ricci flow:

$$w_e^{(t+1)} = w_e^{(t)}(1 - \tau\kappa_e^{(t)}), \quad e = 1, \dots, n, \quad (5)$$

followed by a volume-preserving rescaling. After T iterations we obtain curvature-refined weights $w^{(T)}$.

Curvature-refined anchor affinity. Let $\delta = H^\top \mathbf{1}_m \in \mathbb{R}^n$ denote hyperedge degrees (column sums of H), and define $D_e = \text{diag}(w^{(T)} \oslash \delta)$. We project the refined hypergraph to an anchor affinity

$$S' = HD_eH^\top \in \mathbb{R}^{m \times m}. \quad (6)$$

For efficiency, S' admits a Gram factorization $S' = \tilde{C}^\top \tilde{C}$ with $\tilde{C} = D_e^{1/2} H^\top$, which enables spectral computation in the anchor domain.

Phase-consistent magnetic spectral embedding. To encode cross-view directional tendencies, we augment the refined magnitude backbone S' with a magnetic phase. For each sample s and view v , let $a_s^{(v)} = \arg \max_a C_{a,s}^{(v)}$ be the top-assigned anchor; we map $a_s^{(v)}$ to its global index under the concatenation in C^{mv} . We then accumulate a directed

flow matrix $F \in \mathbb{R}^{m \times m}$ over ordered view pairs:

$$F_{ij} = \sum_{s=1}^n \sum_{v_1 \neq v_2} \mathbb{I}[i = a_s^{(v_1)}, j = a_s^{(v_2)}], \quad \tilde{F} = F - F^\top, \quad (7)$$

and rescale it to a phase matrix

$$\Theta = \beta \frac{\tilde{F}}{\max_{i,j} |\tilde{F}_{ij}| + \epsilon}, \quad \beta = \pi q, \quad q \in (0, 1]. \quad (8)$$

We restrict phases to existing edges of S' and enforce anti-symmetry:

$$\Theta \leftarrow \Theta \odot \mathbb{I}[S' > 0], \quad \Theta \leftarrow \frac{1}{2}(\Theta - \Theta^\top). \quad (9)$$

The complex-valued magnetic adjacency is

$$\tilde{A} = S' \odot \exp(i\Theta), \quad (10)$$

with degree matrix $D_{\tilde{A}} = \text{diag}(|\tilde{A}|\mathbf{1})$ and Hermitian magnetic Laplacian

$$L_{\text{mag}} = I - D_{\tilde{A}}^{-1/2} \tilde{A} D_{\tilde{A}}^{-1/2}. \quad (11)$$

We take the K eigenvectors of L_{mag} with smallest eigenvalues to form an anchor embedding $\Phi_{\text{mag}} \in \mathbb{C}^{m \times K}$ and lift it to samples via

$$M = \text{diag}(\delta)^{-1} H^\top, \quad U_c = M \Phi_{\text{mag}}. \quad (12)$$

Finally, we output a real embedding by concatenating real/imaginary parts and normalizing rows:

$$U = \text{row-norm}([\Re(U_c), \Im(U_c)]) \in \mathbb{R}^{n \times 2K}. \quad (13)$$

Pseudo-labels and spectral self-supervision. Given U , we initialize cluster centers $\{\mu_j\}_{j=1}^K$ by k -means and compute a Student- t soft assignment $Q = [q_{ij}] \in \mathbb{R}^{n \times K}$:

$$q_{ij} = \frac{(1 + \|u_i - \mu_j\|_2^2 / \alpha)^{-(\alpha+1)/2}}{\sum_{j'} (1 + \|u_i - \mu_{j'}\|_2^2 / \alpha)^{-(\alpha+1)/2}}. \quad (14)$$

We then form a sharpened target distribution $P = [p_{ij}]$ to emphasize confident assignments:

$$p_{ij} = \frac{q_{ij}^2 / \sum_{i'} q_{i'j}}{\sum_{j'} q_{ij'}^2 / \sum_{i'} q_{i'j'}}. \quad (15)$$

Let $Q^{(v)}$ denote per-view soft assignments predicted from view-specific representations. We align $\{Q^{(v)}\}_{v=1}^V$ to the shared targets P via

$$\mathcal{L}_{\text{spec}} = \sum_{v=1}^V \text{KL}(P \| Q^{(v)}), \quad (16)$$

which turns the phase-consistent magnetic spectral signal into structured supervision and couples multi-view encoders with the curvature-refined shared geometry.

3.3 Magnetic Laplacian Regularization and Label Consistency Learning

Algorithm 1 Phase-Consistent Magnetic Spectral Learning for MVC

Require: Multi-view data $\{X^{(v)}\}_{v=1}^V$, #clusters K

Ensure: Cluster labels $y \in \{1, \dots, K\}^n$

- 1: Initialize $\{f_\phi^{(v)}, g_\psi^{(v)}\}_{v=1}^V$ (and heads for $Q^{(v)}$ if used).
 - 2: Pretrain autoencoders by minimizing \mathcal{L}_{rec} to obtain $\{Z^{(v)}\}$.
 - 3: For each view v : initialize anchors $A^{(v)}$ by k -means on $Z^{(v)}$, solve (3) to get $C^{(v)}$.
 - 4: Construct anchor hypergraph $(H, w^{(0)})$ from $\{C^{(v)}\}$ and refine weights to $w^{(T)}$ by (5); obtain S' by (6).
 - 5: Build phase Θ from $\{C^{(v)}\}$ and magnetic geometry $(\tilde{A}, L_{\text{mag}})$; compute magnetic spectral embedding U and initialize shared targets P .
 - 6: Lift \tilde{A} to samples and construct L_{cos} (Sec. 3.3).
 - 7: **Stage I: geometry + spectral supervision**
 - 8: **for** epoch = 1 to T_I **do**
 - 9: Compute $\{Q^{(v)}\}$; update networks by minimizing $\mathcal{L}_{\text{rec}} + \lambda_1 \mathcal{L}_{\text{geom}} + \lambda_2 \mathcal{L}_{\text{spec}}$.
 - 10: **(Optional)** periodically refresh geometry and targets.
 - 11: **end for**
 - 12: **Stage II: label contrastive consistency**
 - 13: **for** epoch = 1 to T_{II} **do**
 - 14: Compute $\{Q^{(v)}\}$; update networks by minimizing $\mathcal{L}_{\text{rec}} + \lambda_1 \mathcal{L}_{\text{geom}} + \mathcal{L}_{\text{con}}$.
 - 15: **end for**
 - 16: Recompute U and run k -means on $\{u_i\}_{i=1}^n$ to obtain y .
-

Magnetic-cosine Laplacian smoothing

Let $\tilde{A} \in \mathbb{C}^{m \times m}$ be the curvature-refined magnetic adjacency on anchors (Sec. 3.2), and let $H \in \mathbb{R}^{m \times n}$ be the anchor hypergraph incidence matrix. We build a normalized sample-to-anchor association $M \in \mathbb{R}^{n \times m}$ from H and lift \tilde{A} to the sample level:

$$\delta = H^\top \mathbf{1}_m, \quad M = \text{diag}(\delta)^{-1} H^\top, \quad \tilde{A}^s = M \tilde{A} M^\top. \quad (17)$$

We then form a real-valued magnetic-cosine affinity by combining magnitude and phase:

$$S_{\text{mc}} := \left[|\tilde{A}^s| \odot \cos(\arg(\tilde{A}^s)) \right]_+, \quad D_s := \text{diag}(S_{\text{mc}} \mathbf{1}). \quad (18)$$

where $[\cdot]_+$ denotes element-wise truncation to nonnegative values. The corresponding normalized Laplacian is

$$L_{\text{cos}} = I - D_s^{-1/2} S_{\text{mc}} D_s^{-1/2}. \quad (19)$$

Geometry-aware label regularization. For each view v , let $Q^{(v)} \in \mathbb{R}^{n \times K}$ denote its soft cluster assignments. We regularize $Q^{(v)}$ on the induced sample graph via the Laplacian quadratic form

$$\Omega(Q^{(v)}) = \frac{1}{nK} \text{tr}(Q^{(v)\top} L_{\text{cos}} Q^{(v)}). \quad (20)$$

Together with the anchor-based self-reconstruction and coefficient regularization, we define

$$\mathcal{L}_{\text{geom}}^{(v)} = \|Z^{(v)} - A^{(v)} C^{(v)}\|_F^2 + \gamma \|C^{(v)}\|_F^2 + \lambda_c \Omega(Q^{(v)}), \quad (21)$$

Dataset	V	n	K
100Leaves [Cope <i>et al.</i> , 2013]	3	1600	100
Caltech-5V [Xu <i>et al.</i> , 2022; Li <i>et al.</i> , 2007]	5	1400	7
Digit-Product [Cui <i>et al.</i> , 2024]	2	30000	10
ALOI [Geusebroek <i>et al.</i> , 2005]	4	10800	100
BDGP [Cai <i>et al.</i> , 2012]	2	2500	5
Fashion-MV [Xiao <i>et al.</i> , 2017]	3	10000	10
UCI-3V [Duin, 1998]	3	2000	10
Handwritten [Duin, 1998]	6	2000	10
CUB [Wah <i>et al.</i> , 2011]	2	600	10
Multi-COIL-20 [Nene <i>et al.</i> , 1996]	3	1440	20

Table 2: Dataset statistics. V : number of views; n : number of samples; K : number of clusters.

and aggregate it over views:

$$\mathcal{L}_{\text{geom}} = \sum_{v=1}^V \mathcal{L}_{\text{geom}}^{(v)}. \quad (22)$$

Label contrastive consistency

Cross-view alignment of cluster profiles. Beyond within-view smoothing, different views may still exhibit mismatched cluster semantics; we therefore align cluster profiles across views in the label space to promote cross-view consistency. Let $q_j^{(v)} \in \mathbb{R}^n$ be the j -th column of $Q^{(v)}$. We measure the similarity between two cluster profiles using cosine similarity:

$$\text{sim}(q_j^{(v_1)}, q_k^{(v_2)}) = \frac{\langle q_j^{(v_1)}, q_k^{(v_2)} \rangle}{\|q_j^{(v_1)}\|_2 \|q_k^{(v_2)}\|_2}. \quad (23)$$

For each ordered view pair (v_1, v_2) with $v_1 \neq v_2$ and each cluster index j , we treat $(q_j^{(v_1)}, q_j^{(v_2)})$ as a matched pair and $(q_j^{(v_1)}, q_k^{(v_2)})$ (for $k \neq j$) as mismatched, leading to

$$\mathcal{L}_{\text{con}}^{v_1, v_2} = -\frac{1}{K} \sum_{j=1}^K \log \frac{\exp(\text{sim}(q_j^{(v_1)}, q_j^{(v_2)})/\tau)}{\sum_{k=1}^K \exp(\text{sim}(q_j^{(v_1)}, q_k^{(v_2)})/\tau)}, \quad (24)$$

where $\tau > 0$ is a temperature. Aggregating over all ordered view pairs gives

$$\mathcal{L}_{\text{con}} = \frac{1}{V(V-1)} \sum_{\substack{v_1, v_2=1 \\ v_1 \neq v_2}}^V \mathcal{L}_{\text{con}}^{v_1, v_2}. \quad (25)$$

We optimize the model in a two-stage scheme; the full procedure is summarized in Algorithm 1.

4 Experiments

This section presents overall comparisons with representative classical and recent deep multi-view clustering baselines on diverse benchmarks, followed by component analyses and complementary studies to support the effectiveness of our phase-consistent magnetic spectral signal and the associated learning objectives.

4.1 Experimental Setup

Datasets. We evaluate on ten widely-used multi-view clustering benchmarks summarized in Table 2, covering both object/scene recognition and handwritten/attribute-style recognition tasks. Specifically, 100Leaves and ALOI contain fine-grained object categories with multi-view feature descriptions; Caltech-5V, CUB, and Multi-COIL-20 are multi-view visual recognition benchmarks derived from image datasets; Digit-Product, Fashion-MV, UCI-3V, Handwritten, and BDGP provide complementary settings with different view numbers and cluster granularity. Following common practice, each view is independently normalized by min-max scaling before training.

Baselines. We compare with eight representative baselines, including K-means [MacQueen, 1967] (classical clustering), DEC [Xie *et al.*, 2016] (deep single-view clustering), and recent deep multi-view clustering methods DMCAG [Cui *et al.*, 2023], AEMVC [Li *et al.*, 2025], ALPC [Chen *et al.*, 2025], hubREP [Xu *et al.*, 2025], DCMVC [Cui *et al.*, 2024], and STCMC-UR [Hu *et al.*, 2025]. For each baseline, we use the official implementation (or an author-released reimplementation when applicable) and follow the recommended settings under the same evaluation protocol.

Implementation details. Our model is implemented in PyTorch and optimized with Adam (learning rate 5×10^{-4}). All experiments are conducted on a workstation with two NVIDIA GeForce RTX 5090 GPUs (32 GB each). We set the latent dimension to $z=10$ and follow the two-stage training procedure in Algorithm 1: autoencoder pretraining (1000 epochs), Stage I optimization with $\mathcal{L}_{\text{rec}} + \mathcal{L}_{\text{geom}} + \mathcal{L}_{\text{spec}}$ (1000 epochs), and Stage II refinement with \mathcal{L}_{con} (100 epochs). For anchor-hypergraph construction, we keep top- r assignments per sample with $r=3$. We run Ricci flow for $T_{\text{RF}}=20$ iterations and use the netflow phase scheme with $q=0.25$. Unless otherwise specified, we report the mean performance over 10 random seeds for all methods, including single-view baselines.

4.2 Overall Performance

Table 3 demonstrate that our method achieves the best or second-best performance across ten benchmarks, validating the effectiveness of the proposed phase-consistent magnetic spectral signal. We observe distinct gains on large-scale and heterogeneous datasets (e.g., Fashion-MV, ALOI, and Caltech-5V), confirming that a stable shared signal is crucial for robust cross-view learning under view discrepancy. Even in cases where specific competitors excel, such as DCMVC on 100Leaves, our approach remains a strong runner-up, highlighting its consistent robustness across diverse data distributions. Fig. 3 provides qualitative evidence that our learned representations become more compact and better separated after optimization, while Fig. 4 shows clearer block-diagonal affinity structures with reduced cross-cluster leakage.

Method	Caltech-5V			CUB			UCI-3V			Fashion-MV			Multi-COIL-20		
	ACC	NMI	ARI	ACC	NMI	ARI									
Kmeans	78.51	68.31	61.71	75.83	75.01	61.15	90.05	83.66	80.71	77.84	75.47	68.03	65.48	83.81	63.26
DEC'16	<u>88.64</u>	<u>81.12</u>	81.16	72.67	69.13	53.81	86.65	84.83	80.06	77.85	81.63	71.11	75.01	85.31	70.45
DMCAG'23	83.64	75.41	66.95	67.42	63.64	50.16	85.85	82.26	76.09	84.01	90.12	82.13	99.71	99.68	99.16
AEMVC'25	75.21	66.43	58.32	77.46	76.51	62.72	93.23	91.42	89.71	67.81	55.82	49.21	91.53	94.15	91.31
hubREP'25	68.79	61.31	54.37	67.01	72.45	56.78	83.81	86.56	80.02	73.12	73.61	62.16	68.33	80.32	65.34
ALPC'25	86.29	74.82	84.29	69.83	65.52	49.94	93.55	87.12	85.79	78.34	75.81	68.75	81.24	88.78	77.36
DCMVC'25	86.71	77.78	75.94	<u>78.67</u>	<u>78.27</u>	<u>65.01</u>	96.95	<u>93.41</u>	<u>92.35</u>	91.34	91.19	86.44	75.83	90.33	73.52
STCMC-UR'25	69.34	66.84	45.37	76.31	71.47	56.73	51.24	59.79	36.81	<u>92.32</u>	<u>93.21</u>	<u>87.46</u>	81.76	91.56	77.31
Ours	90.23	82.45	<u>83.45</u>	85.12	81.44	73.45	<u>96.25</u>	93.45	93.65	97.78	94.89	95.21	<u>99.32</u>	<u>98.45</u>	<u>97.23</u>

Method	BDGP			Digit-Product			Handwritten			ALOI			100Leaves		
	ACC	NMI	ARI	ACC	NMI	ARI	ACC	NMI	ARI	ACC	NMI	ARI	ACC	NMI	ARI
Kmeans	46.96	28.69	23.22	66.15	65.26	52.16	78.61	80.49	72.32	55.64	78.52	37.65	85.12	94.31	80.34
DEC'16	93.73	86.31	86.81	74.61	75.56	63.07	93.81	87.57	86.81	53.81	86.45	39.93	82.94	92.12	78.25
DMCAG'23	96.71	92.72	92.25	98.31	95.36	95.82	<u>97.82</u>	<u>95.16</u>	<u>95.27</u>	82.94	88.52	51.31	89.36	94.87	69.52
AEMVC'25	46.43	23.21	17.32	98.16	94.91	95.97	96.95	93.68	93.45	90.23	93.15	84.34	91.43	96.23	89.31
hubREP'25	98.11	<u>95.12</u>	95.23	—	—	—	94.31	88.46	87.87	46.31	68.12	34.21	54.21	78.33	42.41
ALPC'25	<u>88.92</u>	74.64	33.27	69.15	60.68	68.31	94.91	89.41	89.19	79.79	88.94	78.42	—	—	—
DCMVC'25	98.06	96.55	97.42	<u>98.74</u>	<u>96.32</u>	<u>96.12</u>	82.65	88.59	81.11	93.12	96.08	93.48	96.56	99.14	96.33
STCMC-UR'25	74.67	77.61	68.53	94.21	88.58	88.51	87.42	88.65	83.31	21.56	49.32	1.53	32.42	63.56	21.38
Ours	98.81	94.35	<u>95.67</u>	98.89	96.78	96.32	98.35	95.52	95.36	<u>91.36</u>	<u>93.32</u>	<u>84.56</u>	<u>93.21</u>	<u>97.24</u>	<u>92.31</u>

Table 3: **Overall clustering performance (%)**. Rows correspond to datasets and columns correspond to methods. Best results are in **bold** and second-best results are underlined. The symbol “—” indicates that the method failed to yield stable results on the corresponding dataset.

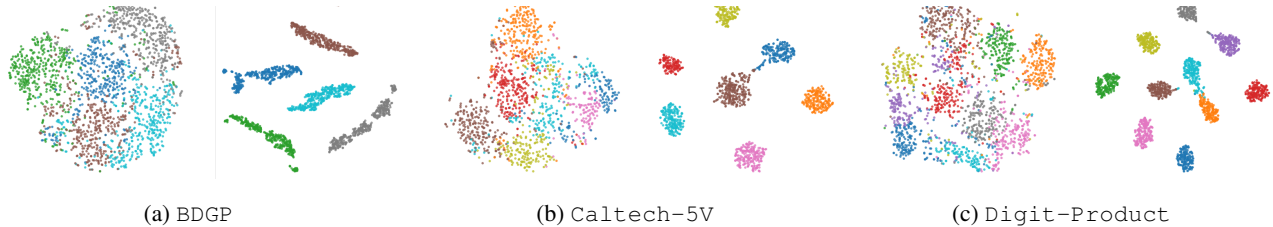


Figure 3: **t-SNE visualizations before vs. after training**. Left/right panels show embeddings before/after training, respectively.

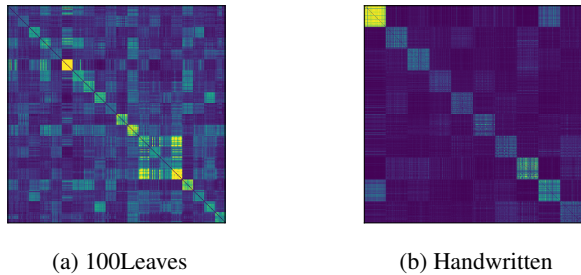


Figure 4: **Affinity heatmaps on two datasets**. Samples are reordered by ground-truth labels to expose block-diagonal structures. Clearer diagonal blocks indicate stronger within-cluster connectivity, while suppressed off-diagonal entries indicate reduced cross-cluster leakage.

4.3 Ablation: Magnetic Spectrum, Phase Causality, and Spectrum Stability

To verify that the gain of our model truly comes from the magnetic spectral mechanism, we conduct a targeted ablation with a simple causal principle: we keep the shared magnitude

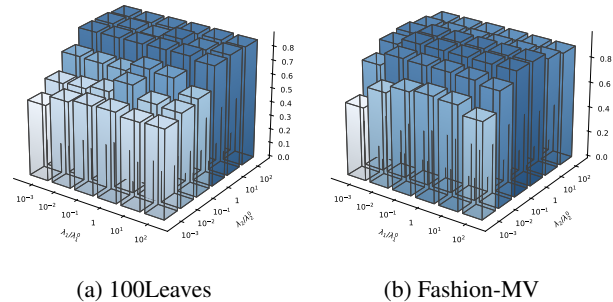


Figure 5: **Stage-I weight sensitivity**. ACC surfaces over (λ_1, λ_2) on (a) 100Leaves and (b) Fashion-MV (axes in log scale).

backbone fixed and only vary the phase/spectral operator.

We first construct the curvature-refined anchor geometry and obtain the shared nonnegative magnitude backbone S' . On top of the same S' , we compare: (i) *Real-Spec* by setting $\Theta = \mathbf{0}$ (equivalently $q=0$) and performing standard real-valued spectral embedding on S' ; (ii) *Mag-Spec (ours)* by

estimating an antisymmetric phase matrix Θ from cross-view assignments and extracting the embedding via the Hermitian magnetic Laplacian on $\hat{A} = S' \odot e^{i\Theta}$; (iii) *Shuffled-Phase*, a counterfactual control that keeps S' unchanged but shuffles the cross-view correspondence used to estimate Θ (e.g., randomly permuting the per-sample top-1 anchor indices across views), yielding Θ_{shuf} ; and optionally (iv) *Random-Phase*, which injects a random antisymmetric phase on the support of S' .

Spectrum stability metrics. We report stability indicators to explain *why* the magnetic spectrum is more robust. *Eigengap* is defined as $\Delta_K = \lambda_{K+1} - \lambda_K$, where $\{\lambda_j\}$ are the eigenvalues (ascending) of the spectral operator; a larger Δ_K typically indicates clearer K -way separation [von Luxburg, 2007]. Moreover, classical perturbation theory (e.g., Davis–Kahan) bounds the deviation of the top- K invariant subspace by the perturbation magnitude scaled by $1/\Delta_K$, implying that larger Δ_K yields a more stable eigenspace [Davis and Kahan, 1970; Stewart and Sun, 1990]. To measure this stability directly, we compute a *subspace distance* across seeds using principal angles: for orthonormal bases $U^{(a)}, U^{(b)} \in \mathbb{R}^{n \times K}$, the singular values of $(U^{(a)})^\top U^{(b)}$ satisfy $\sigma_j = \cos \theta_j$ [Björck and Golub, 1973], and we report $\text{Subspace} = \frac{1}{K} \sum_{j=1}^K \theta_j$ averaged over all run pairs (smaller is better).

Table 4 reports the causal ablation results on three datasets. Across Fashion-MV, BDGP, and Caltech-5V, *Mag-Spec* consistently outperforms *Real-Spec* on ACC/NMI/ARI, and meanwhile yields a larger eigengap Δ_K , a smaller subspace distance (Sub), and a lower k -means inertia (Iner), indicating both clearer spectral separation and more stable/compact embeddings. In contrast, *Shuffled-Phase* and *Random-Phase* markedly degrade all clustering metrics and stability indicators despite using the same magnitude backbone S' , which provides a counterfactual verification that the gain is attributed to *structured, phase-consistent* estimation rather than arbitrary phase injection.

4.4 Complexity and Efficiency

Let n be the number of samples, V the number of views, and m the number of anchors ($m \ll n$). By operating in the anchor domain, constructing sample–anchor assignments and the anchor geometry scales with $O(nm)$, avoiding the $O(n^2)$ cost of dense sample graphs. The spectral signal is extracted on the compact anchor graph (size m) and then lifted to samples via the sample–anchor coefficients, avoiding eigendecomposition on an $n \times n$ matrix. *Real-Spec* performs standard real-valued spectral embedding on the anchor graph (equivalently $\Theta = \mathbf{0}$ or $q=0$), while *Mag-Spec* uses the Hermitian magnetic Laplacian built from the same magnitude backbone and the estimated phase. Table 5 reports the runtime and peak GPU memory on Digit-Product under the same hardware and batch setting.

Overall, the overhead of the magnetic spectrum is moderate, yielding a favorable accuracy–efficiency trade-off.

Dataset / Variant	ACC	NMI	ARI	$\Delta_K \uparrow$	Sub \downarrow	Iner \downarrow
Fashion-MV						
Real-Spec ($q=0$) [†]	95.91	92.72	93.14	0.089	0.46	1.72
Mag-Spec (Ours) [†]	97.78	94.89	95.21	0.125	0.31	1.34
Shuffled-Phase [†]	92.83	88.12	88.91	0.061	0.62	2.15
Random-Phase (Opt.) [†]	92.39	87.52	88.11	0.058	0.66	2.22
BDGP						
Real-Spec ($q=0$) [†]	89.39	84.89	86.48	0.041	0.62	2.48
Mag-Spec (Ours) [†]	98.81	94.35	95.67	0.058	0.44	2.05
Shuffled-Phase [†]	82.08	73.42	70.19	0.026	0.78	2.96
Random-Phase (Opt.) [†]	81.62	72.83	69.61	0.024	0.81	3.02
Caltech-5V						
Real-Spec ($q=0$) [†]	83.20	74.82	71.89	0.036	0.66	2.62
Mag-Spec (Ours) [†]	90.23	82.45	81.45	0.051	0.48	2.18
Shuffled-Phase [†]	79.31	70.11	66.80	0.022	0.82	3.09
Random-Phase (Opt.) [†]	78.94	69.65	66.21	0.021	0.85	3.15

Table 4: Causal ablation under fixed S' on three datasets. Δ_K is eigengap; Sub is subspace distance; Iner is k -means inertia. [†]Prefilled for drafting.

Method	t / epoch (s)	t (min)	GPU (GB)
AG-Base (Real-Spec, $q=0$)	5.8	102	6.1
Full (Mag-Spec)	7.1	125	7.4
STCMC-UR	9.6	168	10.2
DCMVC	8.9	156	9.1

Table 5: **Runtime and memory on Digit-Product.** AG-Base corresponds to Real-Spec ($q=0$), and Full corresponds to Mag-Spec with phase-consistent magnetic spectrum.

4.5 Parameter Sensitivity

Loss-weight balancing. We analyze the sensitivity to the Stage-I loss weights λ_1 and λ_2 for $\mathcal{L}_{\text{geom}}$ and $\mathcal{L}_{\text{spec}}$, respectively, with the reconstruction weight fixed to 1 and Stage II kept at the default setting. We sweep (λ_1, λ_2) on a log-scale grid and report ACC averaged over 10 seeds. As shown in Fig. 5 (a–b), performance is more sensitive to λ_2 and quickly stabilizes once λ_2 reaches a reasonable range, while varying λ_1 causes relatively mild changes. Overall, the broad high-accuracy plateau suggests that our method is robust to loss-weight tuning.

5 Conclusion

Unsupervised multi-view clustering critically depends on a reliable shared structural signal under view discrepancy and noise. We propose *Phase-Consistent Magnetic Spectral Learning* for MVC, which combines a nonnegative magnitude backbone with a phase term encoding directional agreement, extracts a stable shared spectral signal via a Hermitian magnetic Laplacian, and uses it as structured self-supervision for robust learning. Experiments on multiple benchmarks show consistent improvements over strong baselines, and analyses confirm the effectiveness of our key components.

References

- [Arazo *et al.*, 2020] Eric Arazo, Diego Ortego, Paul Albert, Noel E. O’Connor, and Kevin McGuinness. Pseudo-labeling and confirmation bias in deep semi-supervised learning. In *2020 International Joint Conference on Neural Networks (IJCNN)*, pages 1–8. IEEE, 2020.
- [Björck and Golub, 1973] Åke Björck and Gene H. Golub. Numerical methods for computing angles between linear subspaces. *Mathematics of Computation*, 27(123):579–594, 1973.
- [Cai *et al.*, 2012] Xiao Cai, Hao Wang, Heng Huang, and Chris Ding. Joint stage recognition and anatomical annotation of drosophila gene expression patterns. *Bioinformatics*, 28(12):i16–i24, 2012.
- [Chen and Cai, 2011] Xinlei Chen and Deng Cai. Large-scale spectral clustering with landmark-based representation. In *Proceedings of the AAAI Conference on Artificial Intelligence*, 2011.
- [Chen *et al.*, 2023] Jie Chen, Hua Mao, Wai Lok Woo, and Xi Peng. Deep multiview clustering by contrasting cluster assignments. In *Proceedings of the IEEE/CVF International Conference on Computer Vision (ICCV)*, pages 16752–16761, October 2023.
- [Chen *et al.*, 2025] Yawei Chen, Huibing Wang, Jinjia Peng, and Yang Wang. Anchor learning with potential cluster constraints for multi-view clustering. In *Proceedings of the AAAI Conference on Artificial Intelligence (AAAI)*, volume 39, pages 15939–15947, 2025.
- [Chung, 2005] Fan R. K. Chung. Laplacians and the cheeger inequality for directed graphs. *Annals of Combinatorics*, 9(1):1–19, 2005.
- [Cope *et al.*, 2013] J. S. Cope, D. Corney, J. Y. Clark, P. Remagnino, and P. Wilkin. One hundred plant species leaves. UCI Machine Learning Repository, 2013.
- [Cui *et al.*, 2023] Chenhang Cui, Yazhou Ren, Jingyu Pu, Xiaorong Pu, and Lifang He. Deep multi-view subspace clustering with anchor graph. In *Proceedings of the 32nd International Joint Conference on Artificial Intelligence (IJCAI-23)*, pages 3577–3585, 2023.
- [Cui *et al.*, 2024] Jinrong Cui, Yuting Li, Han Huang, and Jie Wen. Dual contrast-driven deep multi-view clustering. *IEEE Transactions on Image Processing*, 33:4753–4764, 2024.
- [Davis and Kahan, 1970] Chandler Davis and W. M. Kahan. The rotation of eigenvectors by a perturbation. III. *SIAM Journal on Numerical Analysis*, 7(1):1–46, 1970.
- [de Resende and Costa, 2020] A. F. de Resende and L. da F. Costa. Magnetic laplacian spectra of directed networks. *Chaos: An Interdisciplinary Journal of Nonlinear Science*, 30(7):073104, 2020.
- [Duin, 1998] Robert P. W. Duin. Multiple features. UCI Machine Learning Repository, 1998.
- [Fang *et al.*, 2023] Uno Fang, Man Li, Jianxin Li, Longxiang Gao, Tao Jia, and Yanchun Zhang. A comprehensive survey on multi-view clustering. *IEEE Transactions on Knowledge and Data Engineering*, 35(12):12350–12368, 2023.
- [Fanuel *et al.*, 2017] Michaël Fanuel, Carlos M. Alaíz, and Johan A. K. Suykens. Magnetic eigenmaps for community detection in directed networks. *Physical Review E*, 95(2):022302, 2017.
- [Feng *et al.*, 2019] Yifan Feng, Haoxuan You, Zizhao Zhang, Rongrong Ji, and Yue Gao. Hypergraph neural networks. In *Proceedings of the AAAI Conference on Artificial Intelligence (AAAI)*, 2019.
- [Fiorini *et al.*, 2023] Stefano Fiorini, Stefano Coniglio, Michele Ciavotta, and Enza Messina. SigMaNet: One laplacian to rule them all. In *Proceedings of the AAAI Conference on Artificial Intelligence (AAAI)*, volume 37, pages 7568–7576, 2023.
- [Gao *et al.*, 2024] Jing Gao, Meng Liu, Peng Li, Jianing Zhang, and Zhikui Chen. Deep multiview adaptive clustering with semantic invariance. *IEEE Transactions on Neural Networks and Learning Systems*, 35(9):12965–12978, 2024.
- [Geusebroek *et al.*, 2005] Jan-Mark Geusebroek, Gertjan J. Burghouts, and Arnold W. M. Smeulders. The amsterdam library of object images. *International Journal of Computer Vision*, 61(1):103–112, 2005.
- [Gu and Wang, 2025] Zhibin Gu and Weili Wang. Hypergraph-enhanced contrastive learning for multi-view clustering with hyper-laplacian regularization. In *The Thirty-ninth Annual Conference on Neural Information Processing Systems*, 2025.
- [Guo *et al.*, 2017] Xifeng Guo, Xinwang Liu, En Zhu, and Jianping Yin. Improved deep embedded clustering with local structure preservation. In *Proceedings of the 26th International Joint Conference on Artificial Intelligence (IJCAI)*, pages 1753–1759, 2017.
- [Hirn *et al.*, 2021] Matthew J. Hirn, Michael Neumann, and Michael T. Schaub. Magnet: A neural network for directed graphs. In *Advances in Neural Information Processing Systems (NeurIPS)*, 2021.
- [Hu *et al.*, 2025] S. Hu, B. Tian, W. Liu, and Y. Ye. Self-supervised trusted contrastive multi-view clustering with uncertainty refined. In *Proceedings of the AAAI Conference on Artificial Intelligence (AAAI)*, 2025.
- [Kang *et al.*, 2020] Zhao Kang, Wenyu Zhou, Qiaolin Zhao, and Zenglin Xu. Multi-graph fusion for multi-view spectral clustering. *Knowledge-Based Systems*, 199:106020, 2020.
- [Kumar *et al.*, 2011] Abhishek Kumar, Piyush Rai, and Hal Daumé III. Co-regularized multi-view spectral clustering. In *Advances in Neural Information Processing Systems (NeurIPS)*, 2011.
- [Li *et al.*, 2007] Fei-Fei Li, Rob Fergus, and Pietro Perona. Learning generative visual models from few training examples: An incremental bayesian approach tested on 101

- object categories. *Computer Vision and Image Understanding*, 106(1):59–70, 2007.
- [Li *et al.*, 2015] Yeqing Li, Feiping Nie, Heng Huang, and Junzhou Huang. Large-scale multi-view spectral clustering via bipartite graph. In *Proceedings of the AAAI Conference on Artificial Intelligence (AAAI)*, pages 2750–2756, 2015.
- [Li *et al.*, 2025] Pengyuan Li, Man Liu, Dongxia Chang, Yiming Wang, Zisen Kong, and Yao Zhao. Aemvc: Mitigate imbalanced embedding space in multi-view clustering. In *Proceedings of the 33rd ACM International Conference on Multimedia (MM '25)*, pages 6461–6470, 2025.
- [Lin and Gao, 2023] Y. Lin and J. Gao. Framelet-magnet: A graph neural network based on framelets and magnetic laplacian. In *Proceedings of the IEEE International Conference on Acoustics, Speech and Signal Processing (ICASSP)*, 2023.
- [Liu *et al.*, 2026] Meng Liu, Yuzhe Li, Zhikui Chen, and Yilong Lin. Information-driven complementarity and consistency mining for multi-view clustering. *IEEE Signal Processing Letters*, 33:216–220, 2026.
- [MacQueen, 1967] J. MacQueen. Some methods for classification and analysis of multivariate observations. In *Proceedings of the Fifth Berkeley Symposium on Mathematical Statistics and Probability*, volume 1, pages 281–297, 1967.
- [Nene *et al.*, 1996] Sameer A. Nene, Shree K. Nayar, and Hiroshi Murase. Columbia object image library (coil-20). Technical Report CUCS-005-96, Department of Computer Science, Columbia University, 1996.
- [Ni *et al.*, 2019] C. Ni, Y. Lin, and J. Gao. Network alignment by discrete ollivier-ricci flow. In *Graph Drawing and Network Visualization*. Springer, 2019. GD 2018 proceedings; update LNCS volume/pages if you want.
- [Ollivier, 2009] Yann Ollivier. Ricci curvature of Markov chains on metric spaces. *Journal of Functional Analysis*, 256(3):810–864, 2009.
- [Pan *et al.*, 2021] En Pan, Jie Xu, Yazhou Ren, Ce Zhu, and Dacheng Tao. Multi-view contrastive graph clustering. In *Advances in Neural Information Processing Systems (NeurIPS)*, 2021.
- [Sia *et al.*, 2019] J. Sia, E. Jonckheere, and P. Bogdan. Ollivier-Ricci curvature-based method to community detection in complex networks. *Scientific Reports*, 9, 2019.
- [Singer and Wu, 2012] Amit Singer and Hau-Tieng Wu. Vector diffusion maps and the connection laplacian. *Communications on Pure and Applied Mathematics*, 65(8):1067–1144, 2012.
- [Stewart and Sun, 1990] G. W. Stewart and Ji-Guang Sun. *Matrix Perturbation Theory*. Academic Press, Boston, 1990.
- [von Luxburg, 2007] Ulrike von Luxburg. A tutorial on spectral clustering. *Statistics and Computing*, 17(4):395–416, 2007.
- [Wah *et al.*, 2011] Catherine Wah, Steve Branson, Peter Welinder, Pietro Perona, and Serge Belongie. The caltech-ucsd birds-200-2011 dataset. Technical Report CNS-TR-2011-001, California Institute of Technology, 2011.
- [Wang *et al.*, 2025] Bocheng Wang, Chusheng Zeng, Mulin Chen, and Xuelong Li. Towards learnable anchor for deep multi-view clustering. In *Proceedings of the AAAI Conference on Artificial Intelligence*, 2025.
- [Xiao *et al.*, 2017] Han Xiao, Kashif Rasul, and Roland Vollgraf. Fashion-mnist: a novel image dataset for benchmarking machine learning algorithms. *arXiv preprint arXiv:1708.07747*, 2017.
- [Xie *et al.*, 2016] Junyuan Xie, Ross Girshick, and Ali Farhadi. Unsupervised deep embedding for clustering analysis. In *Proceedings of the 33rd International Conference on Machine Learning (ICML)*, pages 478–487, 2016.
- [Xu *et al.*, 2022] Jie Xu, Huayi Tang, Yazhou Ren, Liang Peng, Xiaofeng Zhu, and Lifang He. Multi-level feature learning for contrastive multi-view clustering. In *Proceedings of the IEEE/CVF Conference on Computer Vision and Pattern Recognition (CVPR)*, 2022.
- [Xu *et al.*, 2024] Jie Xu, Yazhou Ren, Xiaolong Wang, Lei Feng, Zheng Zhang, Gang Niu, and Xiaofeng Zhu. Investigating and mitigating the side effects of noisy views for self-supervised clustering algorithms in practical multi-view scenarios. In *Proceedings of the IEEE/CVF Conference on Computer Vision and Pattern Recognition (CVPR)*, pages 22957–22966, June 2024.
- [Xu *et al.*, 2025] Zheming Xu, He Liu, Congyan Lang, Tao Wang, Yidong Li, and Michael C. Kampffmeyer. A hubness perspective on representation learning for graph-based multi-view clustering. In *Proceedings of the IEEE/CVF Conference on Computer Vision and Pattern Recognition (CVPR)*, pages 15528–15537, June 2025.
- [Zeng *et al.*, 2026] Chusheng Zeng, Bocheng Wang, Mulin Chen, Zechao Li, and Xuelong Li. Hypergraph regularization-based anchor learning for multi-view clustering. *Pattern Recognition*, 172:112465, 2026.
- [Zhang *et al.*, 2024] Chao Zhang, Xiuyi Jia, Zechao Li, Chunlin Chen, and Huaxiong Li. Learning cluster-wise anchors for multi-view clustering. In *Proceedings of the AAAI Conference on Artificial Intelligence*, pages 16696–16704, 2024.
- [Zhou *et al.*, 2006] Dengyong Zhou, Jiayuan Huang, and Bernhard Schölkopf. Learning with hypergraphs: Clustering, classification, and embedding. In *Advances in Neural Information Processing Systems*, 2006.
- [Zhou *et al.*, 2024] Lihua Zhou, Guowang Du, Kevin Lü, Lizheng Wang, and Jie Du. A survey and an empirical evaluation of multi-view clustering approaches. *ACM Computing Surveys*, 2024.